A comparison of Neutral Atom Detector Unit neutral atom image inversion with a comprehensive ring current model

C. L. Tang,[1] L. Lu,[2] S. McKenna-Lawlor,[3] S. Barabash,[4] Z. X. Liu,[2] M.-C. Fok,[5] and Z. Y. Li[1]

Received 23 July 2007; revised 19 November 2007; accepted 21 December 2007; published 30 May 2008.

[1] We present energetic neutral atom (ENA) images in the energy range 45 to 50 keV for H and 92 to 138 keV for O measured by the Neutral Atom Detector Unit (NUADU) onboard Double Star TC-2 during a geomagnetic storm on 8 May 2005. We compare the ion fluxes deduced from inversion of the NUADU image with those calculated using the Comprehensive Ring Current Model (CRCM). This comparison shows that the two approaches are consistent when used to derive the configuration of the corresponding global ion distribution and the peak ion fluxes. The deduced peak ion flux is located in the premidnight sector at 1540 UT, while the deduced ion peak flux is located in the midnight sector at 1610 UT. There are strong ion fluxes in the region between $L = 2$ and $L = 4$ which form a closed loop configuration. The ion peak flux is about 2.2×10^6/cm^2/sr/keV/s. The deduced ion distribution agrees well with the NUADU measurement. The agreement between the inverted ion distributions and the CRCM results give us confidence in applying our ENA imaging and modeling techniques to the study of the evolution of the inner magnetosphere plasma distribution and the global dynamics of the ring current during magnetic storms.

Citation: Tang, C. L., L. Lu, S. McKenna-Lawlor, S. Barabash, Z. X. Liu, M.-C. Fok, and Z. Y. Li (2008), A comparison of Neutral Atom Detector Unit neutral atom image inversion with a comprehensive ring current model, *J. Geophys. Res.*, *113*, A07S32, doi:10.1029/2007JA012680.

1. Introduction

[2] Energetic neutral atom (ENA) imaging in the magnetosphere relies on charge-exchange interactions between energetic ions and cold atoms in the neutral geocorona and upper atmosphere. These interactions give rise to the production of energetic neutral atoms (ENAs) which propagate unconstrained by magnetic and electric fields and therefore can be used to remotely image the ring current and plasma sheet using instruments such as the Neutral Atom Detector Unit (NUADU) aboard the Double Star TC-2 satellite [*McKenna-Lawlor et al.*, 2004]. ENA images thus contain global information about magnetosphere-exosphere interactions. The count rate characterizing each pixel of an ENA image is determined by the line of sight integral (along the line of sight direction of the pixel) of the unidirectional ion fluxes multiplied by the local density of the neutral exospheric gas and by the particle charge exchange cross sections [*Roelof*, 1987]. These count rates depend on the viewing angle and altitude of the satellite. Thus, the extraction from an ENA image of quantitative information regarding the parent ion distributions (which are a function of circumstances relating to the energetic ion and cold neutral distributions) requires special ENA inversion technique [*Roelof and Skinner*, 2000; *Perez et al.*, 2000, 2001; *C:son Brandt et al.*, 2002; L. Lu et al., Iterative inversion of global magnetospheric ion distributions using energetic neutral atom (ENA) images recorded by the NUADU/TC2 instrument, submitted to *Annales Geophysicae*, 2008].

[3] A comprehensive ring current model (CRCM) can simulate, using a self-consistent calculated electric field, the evolution of the plasma distribution in the inner magnetosphere conserving the first two adiabatic invariants [*Fok et al.*, 2001]. ENA simulations made using CRCM were found by *Fok et al.* [2003] to successfully explain certain previously puzzling features present in a number of events recorded by the HENA instrument on IMAGE.

[4] To demonstrate the validity of a new inversion method recently developed using NUADU ENA data to reconstruct ion distributions in the inner magnetosphere (Lu et al., submitted manuscript, 2008), ion fluxes calculated with the CRCM model are compared in this paper to those inferred from ENA image inversions in the energy range 45 to 50 keV for H and 92 to 138 keV for O. The results indicate that the two approaches yield consistent configu-

[1]School of Earth and Space Sciences, University of Science and Technology of China, Hefei, China.
[2]Centre for Space Science and Applied Research of the Chinese Academy of Sciences, Beijing, China.
[3]Space Technology Ireland, National University of Ireland, Maynooth, Ireland.
[4]Swedish Institute of Space Physics, Kiruna, Sweden.
[5]NASA Goddard Space Flight Center, Greenbelt, Maryland, USA.

Copyright 2008 by the American Geophysical Union.
0148-0227/08/2007JA012680

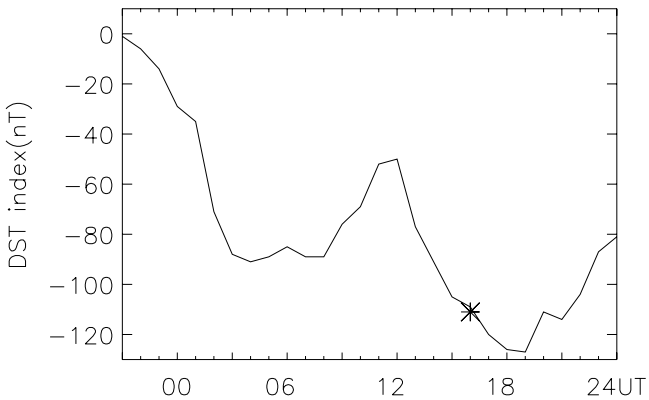

Figure 1. The development of the *Dst* index on 8 May 2005. During 1540–1615 UT when ENA measurements were taken, *Dst* index was about −110 nT (marked by an asterisk).

rations for the global ion distribution and for the magnitude of the ion peak flux.

2. Observations

2.1. Storm on 8 May 2005

[5] Geomagnetic indices, as shown in Figure 1 for *Dst*, indicate that the magnetosphere was highly disturbed during the 8 May 2005 event, with $Kp = 8^+$ and $Dst \sim -127$ nT. Near the peak of the storm at 1540 UT and 1610 UT, ENA measurements were taken from the TC-2 satellite. Figure 2 shows a plot of the 50–75 keV proton fluxes measured by the Synchronous Orbit Particle Analyzer (SOPA) on board the Los Alamos National Laboratory (LANL) 1994–084 satellite during this period. From about 1200 to 1800 UT, the ion fluxes at geosynchronous orbit are enhanced over the period prior to and following this interval. The 1994–084 satellite was located between 0000 and 0050 MLT during the 1200–1800 UT interval.

2.2. ENA Observations

[6] Figure 3 shows the ENA images recorded in energy channel 1 (45 to 50 keV for H, 92 to 138 keV for O) of the NUADU instrument [*McKenna-Lawlor et al.*, 2004] at 1540 UT (from 1537:59 to1542:37 UT) and 1610 UT (from 1607:30 to 1612:09 UT) during the storm main phase on 8 May 2005 (integration time about 5 min). During the big storm, ENA signatures could be identified in data recorded during each spacecraft spin but, in the smoothing process, the accumulation time for each pixel in Figure 3 was 2.17 s. The ENA image is presented in an azimuthal equidistant projection and it is noted that it was precleaned to remove the effect of the sun pulse, and differences in responses between the detectors. NUADU measurements, which show a strong asymmetry, are characterized by an enhancement in the premidnight section at 1540 UT. Half an hour later at 1610 UT, the ENA enhancement region has drifted to midnight. The ENA count distributions of the ENA count maximum and its ambient azimuth/elevation of the image are shown in Figure 4 (where the top panels show the azimuth/elevation at 1540 UT and the bottom panels at 1610 UT), where the maximum count is about 2500, and the average noise background is about 250. This is discounted as noise background during inversion process. The standard deviation is about 110 for this event. It is clear from Figure 4 that NUADU barely detected the ring current above noise for this event. This has often been a challenge for ENA observations. The average noise background was corrected through a modification term in efficiency coefficients of the detector response function statistically, and fluctuations were mainly smoothed by constraint factor during inversions.

3. Simulation

[7] *Fok et al.* [2003] performed ring current simulations based on a kinetic model developed by *Fok and Moore* [1997] and *Fok et al.* [1999]. The boundary of this model was taken to be at $\sim 1\ R_E$ inside the magnetopause on the dayside and at 10/12 R_E equatorial distance on the nightside. In a test simulation of ring current development during a major storm, it was assumed by *Fok et al.* [2003] that the distribution on the nightside boundary was uniform over local time and approximated by a Maxwellian with density (n) and temperature (T) which was given (following *Borovsky et al.* [1998] and *Ebihara and Ejiri* [2000]) by:

$$n(t)\left[cm^{-3}\right] = 0.395 + 0.025 \cdot n_{sw}(t - 3\text{hr})$$

$$T(t)[\text{keV}] = -3.65 + 0.019 \cdot \nu_{sw}(t - 3\text{hr})$$

where n_{sw} and ν_{sw} are respectively the solar wind density (in cm^{-3}) and velocity (in km s^{-1}) at the dayside magnetopause. The plasma sheet distribution was represented by the solar wind conditions on the dayside with a delay time of 3 h (the approximate time required for solar wind effects to propagate to the inner plasma sheet). The Tsyganenko magnetic field model [*Tsyganenko*, 1995; *Tsyganenko and Stern*, 1996], an empirical model for the convection electric field [*Weimer*, 1995] and the self consistent field output from the Comprehensive Ring Current Model (CRCM) of *Fok et al.* [2001] were used in this ring current simulation. In brief overview, the Rice Convection Model/RCM [*Harel et al.*, 1981] serves as an electric field solver in the CRCM while the Fok ring current

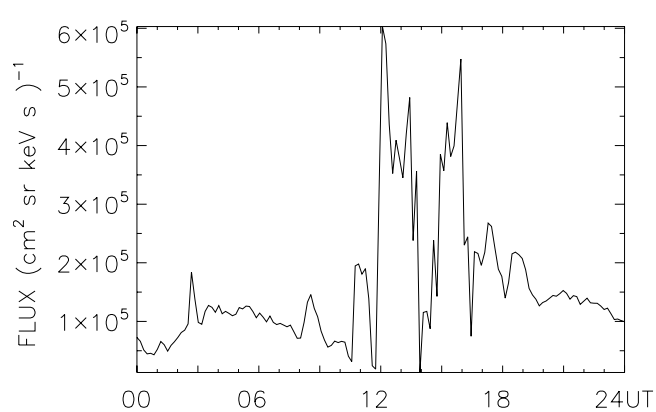

Figure 2. The 50–75 keV protons fluxes measured at the geostationary orbit by SOPA on board the LANL1994–084 spacecraft, between 0000 and 2400 UT.

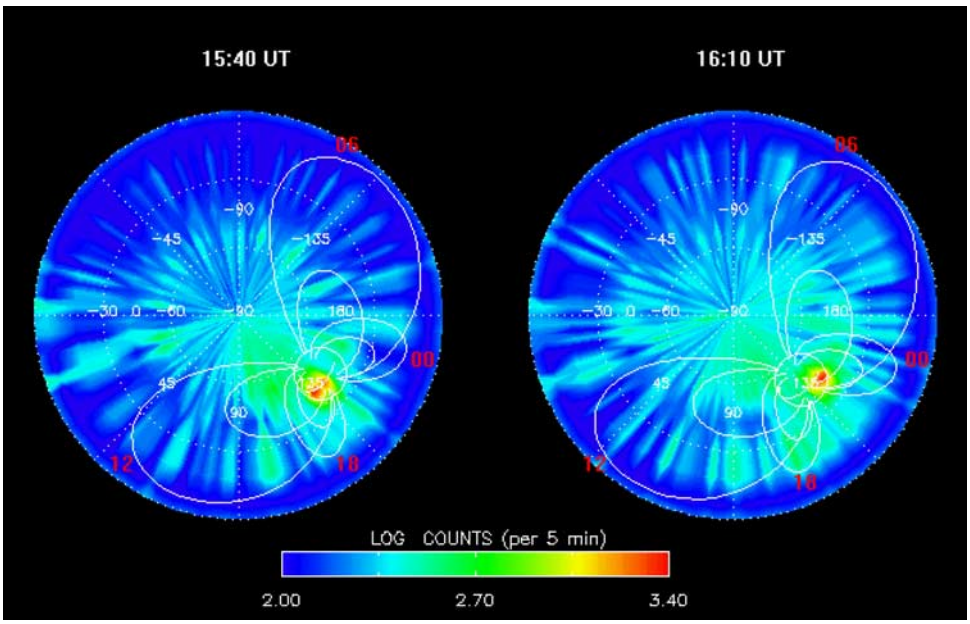

Figure 3. ENA image recorded at 1540 UT (from 1537:59 to1542:37 UT) and 1610 UT (from 1607:30 to 1612:09 UT) on 8 May 2005, in NUADU energy channel 1. The color scales indicate the number of particle counts in each pixel. The magnetic dipole field lines of L shells 4 and 8 are drawn for reference at noon, dawn, midnight, and dusk. The magnetic local time (MLT) of each set of field lines is given in red.

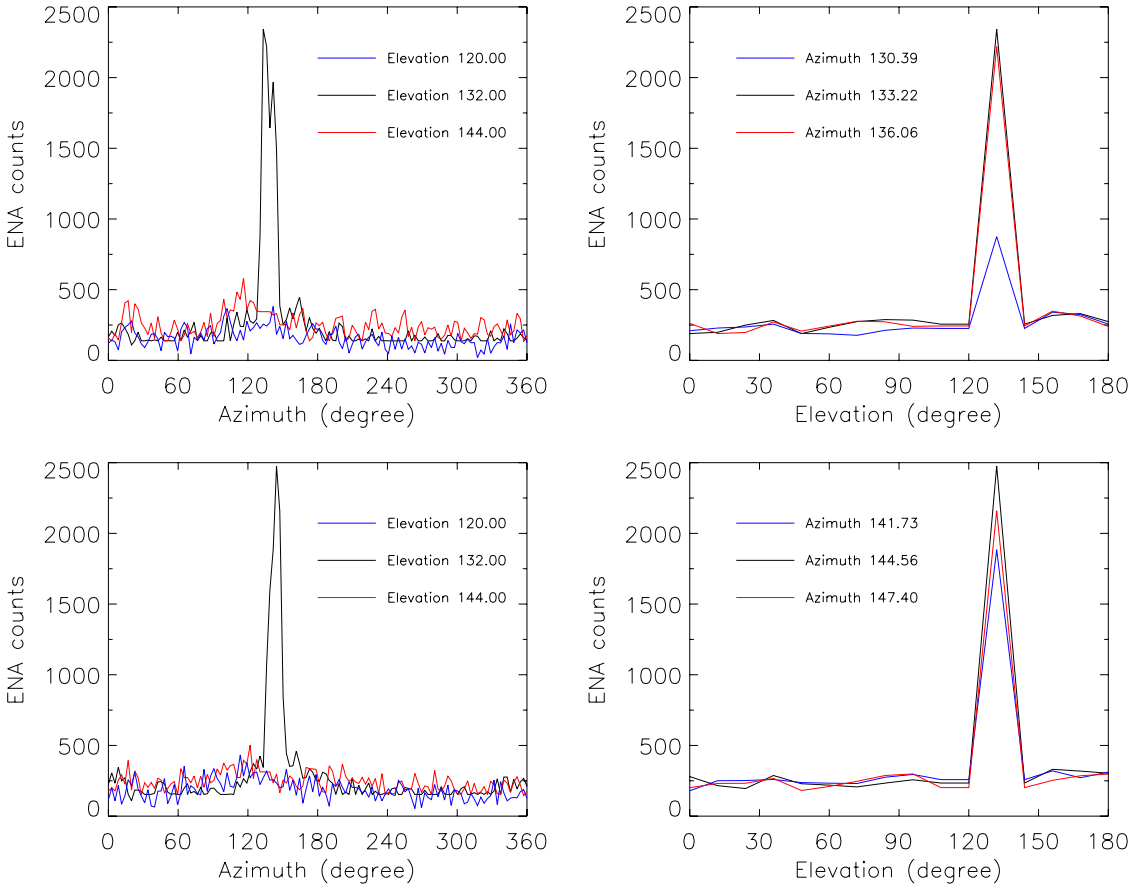

Figure 4. The ENA count distributions of the azimuth and the elevation at (top) 1540 UT and (bottom) 1610 UT on 8 May 2005, where black curves are for the ENA maximum and red and blue curves are the ENA count with azimuth/elevation ambient the ENA maximum.

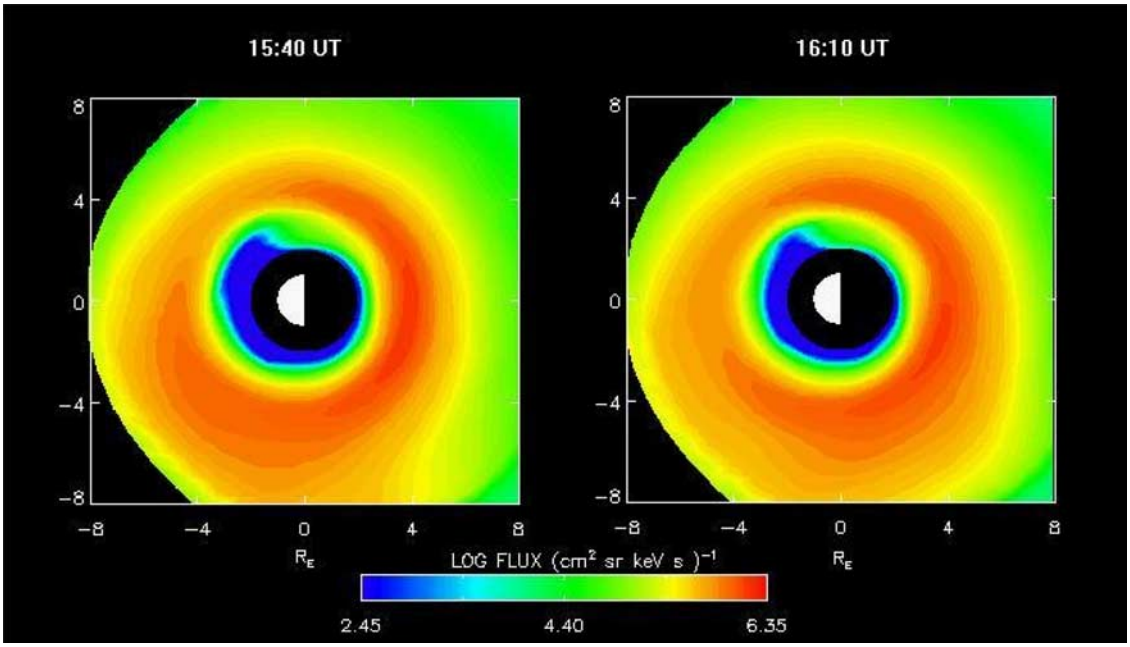

Figure 5. Simulated 45–50 keV proton flux averaged over all pitch angles at the equator at 1540 UT and 1610 UT on 8 May 2005.

model [*Fok and Moore*, 1997] plays the role of a particle tracer. The ring current model calculates plasma differential fluxes that vary with time, energy, pitch angle and location in three-dimensional spatial space [*Fok et al.*, 2003].

[8] The ring current development during the magnetic storm of 8 May 2005 is simulated here using the electric field approximated by the CRCM [*Fok et al.*, 2001]. Figure 5 shows the simulated fluxes in the energy range 45 to 50 keV for protons averaged over all pitch angles at the equator at 1540 UT and 1610 UT on 8 May 2005. Note that for the equatorial ion flux plot, the Sun is to the left and dawn is up. The peak of the ion fluxes is seen to be located in the premidnight at 1540 UT, while the simulated ion peak flux is located in the midnight sector at 1610 UT. In the region between $L = 2$ and $L = 4$, a ring current configuration is developing. The simulated ion peak flux magnitude is 1.6×10^5/cm^2/sr/keV/s in the energy range 92 to 138 keV for oxygen ions (not plotted).

4. Inversion

[9] The inversion technique for the ENA data recorded by the NUADU instrument is described in detail by Lu et al. (submitted manuscript, 2008). NUADU does not discriminate different species of ENAs. The mixing ratio between the hydrogen and oxygen present in the energy range of NUADU can be estimated by determining the hydrogen to oxygen ion flux magnitude ratio using CRCM. For example it is inferred that the hydrogen ENA flux is about 12 times higher than the oxygen ENA flux in the first energy channel (45–50 keV range) for H and also in the 92–138 keV range for O during the geomagnetic storm of 8 May 2005. Thus, we will obtain a mixed ion flux distribution (12:1 ratio between hydrogen and oxygen).

[10] When the parameter gamma γ (which is the constraint strength for the constrained inversion method, see also *DeMajistre et al.* [2004]) is taken to be about 0.02, the relative error (determined by comparing the recovered image with measurement pixel by pixel) attains a minimum (at <0.2). We thereby obtain the optimal equatorial ion distribution shown in Figure 6. Here, the peak of the ion flux is located in the premidnight at 1540 UT,while the deduced ion peak flux is located in the midnight sector at 1610 UT. In the region between $L = 2$ and $L = 4$, a ring current configuration is developing. The ion peak flux is about 2.2×10^6/cm^2/sr/keV/s.

[11] Using the deduced ion distribution, the optimal simulated image (Figure 7) is recovered in the same format as that in Figure 3. The asymmetry in local time of the deduced ion distribution is also visible in the optimal simulated ENA image. The overall distribution in local time seen in the optimal simulated image is consistent with the NUADU measurements. The deduced ion distribution thus agrees well with the NUADU measurement. In Figure 3, NUADU measurements, which show a strong asymmetry, are characterized by an enhancement in the premidnight section at 1540 UT. This local time asymmetry is also apparent in the deduced ion distribution. The peak of the deduced ion flux is located in the premidnight sector (Figure 6). The following picture of the storm time ring current at 1540 agrees with the commonly held view: Energetic particles are first injected on the nightside. When they encounter the inner region of the magnetosphere and its associated strong magnetic field, they drift westward toward dusk, and the ion flux peak consequently appears in the premidnight sector. Half an hour later at 1610 UT, the ENA enhancement region has drifted to midnight, and the deduced ion peak flux is also located in the midnight sector. At 1610 UT, the convection electric field becomes deformed, which may be related to the enhanced plasma sheet density. The high plasma sheet density increases the region 2 field-aligned current, strengthening the eastward directed shielding electric field [*Ebihara and Fok*, 2004]. The ion flux peak then shifts from the nightside toward dawn. Note, however, that there are probably other mechanisms that

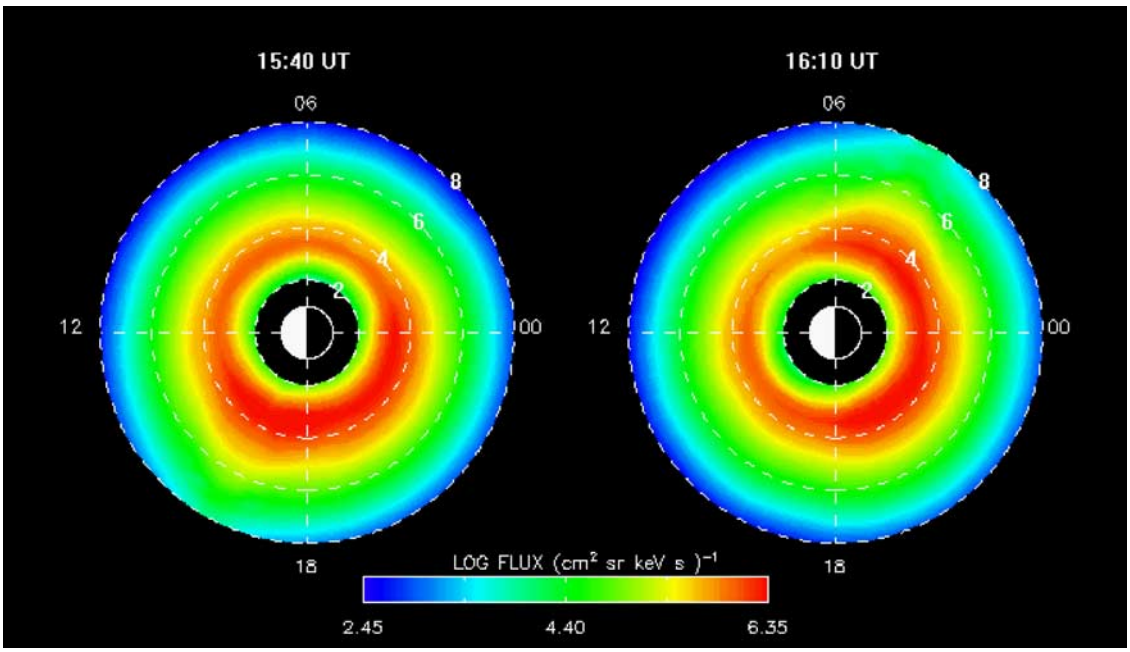

Figure 6. Optimal equatorial ion distribution obtained using constrained linear inversion averaged over all pitch angles, where the dashed contours represent the shells L (2–8) in Earth radii and the local timescale is provided outside the perimeter of the outermost L boundary.

can also explain the time variation in the region of enhanced ion fluxes.

5. Discussion

[12] The ion fluxes deduced from the inversion of NUADU ENA data were compared with those simulated using the electric field approximated by the CRCM. The results show that the two approaches yield consistent results in deriving the global ion distribution configuration (in each case the peak of the ion flux is located in the premidnight at 1540 UT, while the deduced ion peak flux is located in the midnight sector at 1610 UT). A ring current configuration was shown to be located in the region between $L = 2$ and

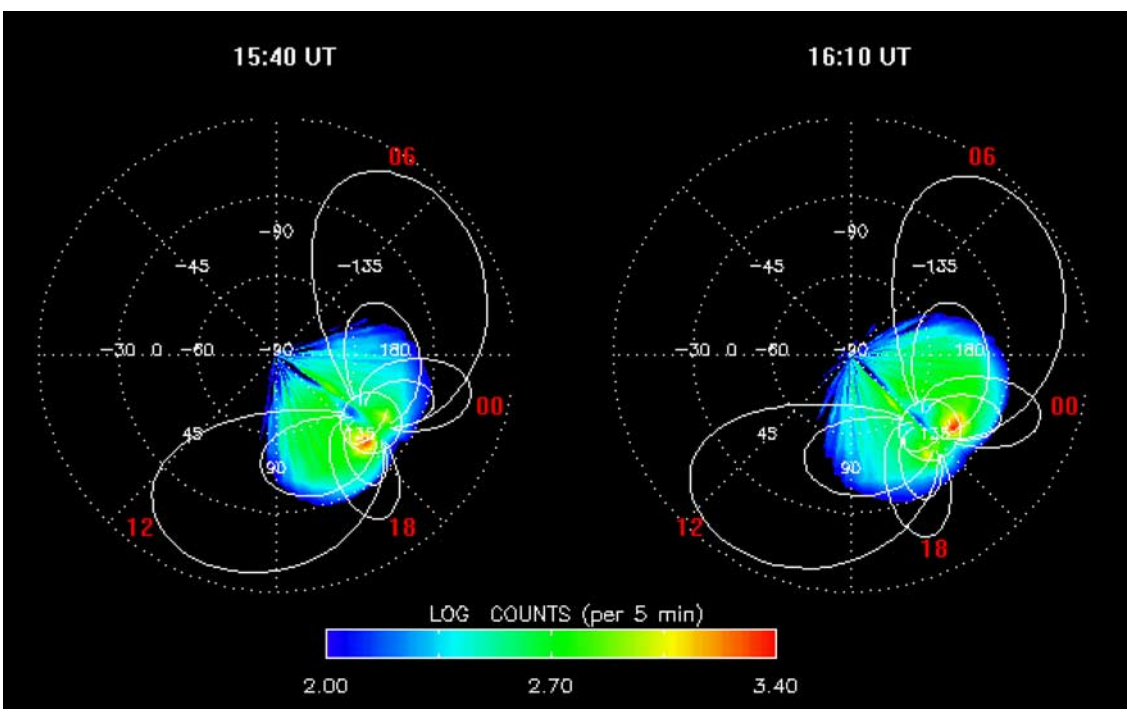

Figure 7. Optimal simulated ENA image displayed in the same format used in Figure 3 based on constrained linear inversion.

$L = 4$. The simulated ion peak flux magnitude is 1.9×10^6/cm^2/sr/keV/s in the energy range 45 to 50 keV for protons, and the simulated ion peak flux magnitude is 1.6×10^5/cm^2/sr/keV/s in the energy range 92 to138 keV for oxygen ions. Using constrained linear inversion, the ion peak flux magnitude was estimated to be 2.2×10^6/cm^2/sr/keV/s for the optimal equatorial ion distribution (Figure 6) with a 12:1 ratio between hydrogen and oxygen. Seen from above, the inverted ion peak flux magnitude is consistent with that from the CRCM simulation.

[13] The simulated ion flux is stronger than the NUADU inverted flux at $L > 5$. This may be a consequence of the influence of the viewing angle and altitude of the satellite. Note that the image was taken over the North Pole, at a time the TC-2 satellite was at GSM position [3.43 $\sim$ 3.15, $-3.95 \sim -3.45$, 2.86 $\sim$ 2.94] R_E. Instrumental factors can also play a role since the NUADU instrument is essentially a remote-sensing camera. The inversions in this study assumed a simple dipolar magnetic field model which would introduce a slight shift in the radial location of the resulting ion distribution.

[14] The comparison between the simulated ion fluxes using the CRCM and those deduced from ENA image inversion yield consistent global ion distributions and ion peak fluxes, despite the inherent influence of dispersion. To obtain more detailed ion distributions, it will be necessary to utilize simultaneous measurements from several satellites.

6. Conclusion

[15] We used as an example case the magnetic storm of 8 May 2005 to compare simulated ion fluxes derived using CRCM with distributions deduced from the inversion of recorded Double Star TC-2 ENA images.

[16] In the main phase of the magnetic storm on 8 May 2005, we found that:

[17] 1. ENA emissions in the energy range 45 to 50 keV for H and 92 to 138 keV for O displayed a pre-midnight enhancement at 1540 UT. Half an hour later at 1610 UT, the ENA enhancement region had drifted to midnight.

[18] 2. The deduced ion peak flux was located in the premidnight at 1540 UT, while the deduced ion peak flux was located in the midnight sector at 1610 UT in the region between $L = 2$ and $L = 4$, which was characterized by the presence of a ring current. The ion peak flux was about 2.2×10^6/cm^2/sr/keV/s. The ion distribution inferred compared favorably to the NUADU data.

[19] 3. The comparisons show that the two approaches agree in their determinations of both the configuration of the global ion distribution and the ion peak flux magnitude.

[20] This agreement indicates that we can confidently apply our imaging and simulation techniques to further study the evolution of the inner magnetosphere plasma distributions and the global dynamics of ring current during magnetic storms.

[21] **Acknowledgments.** The *Dst* index was provided from the World Data Center for Geomagnetism, Kyoto. We are also grateful to G. Reeves at the Los Alamos National Laboratory for supplying digital SOPA data. This study was supported by the Chinese National Natural Science Foundation Committee grants and 4039015340674083.

[22] Zuyin Pu thanks the reviewers for their assistance in evaluating this paper.

References

Borovsky, J. E., M. F. Thomsen, and R. C. Elphic (1998), The driving of the plasma sheet by the solar wind, *J. Geophys. Res.*, *103*, 17,617–17,639, doi:10.1029/97JA02986.

C:son Brandt, P., R. Demajistre, E. C. Roelof, D. G. Mitchell, and S. Mende (2002), IMAGE/high-energy energetic neutral atom: Global energetic neutral atom imaging of the plasma sheet and ring current during substorms, *J. Geophys. Res.*, *107*(A12), 1454, doi:10.1029/2002JA009307.

DeMajistre, R., E. C. Roelof, P. C. Brandt, and D. G. Mitchell (2004), Retrieval of global magnetospheric ion distributions from high-energy neutral atom measurements made by the IMAGE/HENA instrument, *J. Geophys. Res.*, *109*, A04214, doi:10.1029/2003JA010322.

Ebihara, Y., and M. Ejiri (2000), Simulation study on fundamental properties of the storm-time ring current, *J. Geophys. Res.*, *105*, 15,843–15,859, doi:10.1029/1999JA900493.

Ebihara, Y., and M.-C. Fok (2004), Postmidnight storm-time enhancement of tens-of-keV proton flux, *J. Geophys. Res.*, *109*, A12209, doi:10.1029/2004JA010523.

Fok, M.-C., and T. E. Moore (1997), Ring current modeling in a realistic magnetic field configuration, *Geophys. Res. Lett.*, *24*, 1775–1778, doi:10.1029/97GL01255.

Fok, M.-C., T. E. Moore, and D. C. Delcourt (1999), Modeling of inner plasma sheet and ring current during substorms, *J. Geophys. Res.*, *104*, 14,557–14,569, doi:10.1029/1999JA900014.

Fok, M.-C., R. A. Wolf, R. W. Spiro, and T. E. Moore (2001), Comprehensive computational model of the Earth's ring current, *J. Geophys. Res.*, *106*, 8417–8424, doi:10.1029/2000JA000235.

Fok, M.-C., T. E. Moore, G. R. Wilson, J. D. Perez, X. X. Zhang, P. C:son Brandt, D. G. Mitchell, E. C. Roelof, M. J.-Jahn, C. J. Pollock, and R. A. Wolf (2003), Global ENA image simulations, *Space Sci. Rev.*, *109*, 77–103, doi:10.1023/B:SPAC.0000007514.56380.fd.

Harel, M., R. A. Wolf, P. H. Reiff, R. W. Spiro, W. J. Burke, F. J. Rich, and M. Smiddy (1981), Quantitative simulation of a magnetospheric substorm, 1, Model logic and overview, *J. Geophys. Res.*, *86*, 2217–2241, doi:10.1029/JA086iA04p02217.

McKenna-Lawlor, S., et al. (2004), The energetic NeUtral Atom Detector Unit (NUADU) for China's Double Star Mission and its calibration, *Nucl. Instrum. Methods A*, *503*, 311–322.

Perez, J. D., C. M.-Fok, and T. E. Moore (2000), Deconvolution of energetic neutral atom images of the Earth's magnetosphere, *Space Sci. Rev.*, *91*, 421–436, doi:10.1023/A:1005277307611.

Perez, J. D., G. Kozlowski, P. C. Brandt, D. G. M. Itchell, J. M. Jahn, C. J. Pollock, and X. Zhang (2001), Initial ion equatorial pitch angle distributions from energetic neutral atom images obtained by IMAGE, *Geophys. Res. Lett.*, *28*, 1155–1158, doi:10.1029/2000GL012636.

Roelof, E. C. (1987), Energetic neutral atom image of a storm-time ring current, *Geophys. Res. Lett.*, *14*, 652–655, doi:10.1029/GL014i006p00652.

Roelof, E. C., and A. J. Skinner (2000), Extraction of ion distributions from magnetospheric ENA and EUV images, *Space Sci. Rev.*, *91*, 437–459, doi:10.1023/A:1005281424449.

Tsyganenko, N. A. (1995), Modeling the Earth's magnetospheric magnetic field confined within a realistic magnetopause, *J. Geophys. Res.*, *100*, 5599–5612, doi:10.1029/94JA03193.

Tsyganenko, N. A., and D. P. Stern (1996), Modeling the global magnetic field of the large-scale Birkeland current systems, *J. Geophys. Res.*, *101*, 27,187–27,198, doi:10.1029/96JA02735.

Weimer, D. R. (1995), Models of high-latitude electric potentials derived with a least error fit of spherical harmonic coefficients, *J. Geophys. Res.*, *100*, 19595–19607, doi:10.1029/95JA01755.

S. Barabash, Swedish Institute of Space Physics, SE-98128 Kiruna, Sweden.

M.-C. Fok, NASA Goddard Space Flight Center, Greenbelt, MD 20771, USA.

Z. Y. Li and C. L. Tang, School of Earth and Space Sciences, University of Science and Technology of China, Hefei, 230026, China. (tcl@mail.ustc.edu.cn)

Z. X. Liu and L. Lu, Centre for Space Science and Applied Research of the Chinese Academy of Sciences, 100081 Beijing, China.

S. McKenna-Lawlor, Space Technology Ireland, National University of Ireland, Maynooth, Ireland.